New Journal of Physics
The open access journal at the forefront of physics

Deutsche Physikalische Gesellschaft DPG IOP Institute of Physics

The temperature-dependent magnetization profile across an epitaxial bilayer of ferromagnetic $La_{2/3}Ca_{1/3}MnO_3$ and superconducting $YBa_2Cu_3O_{7-\delta}$

To cite this article: S Brück *et al* 2011 *New J. Phys.* **13** 033023

New Journal of Physics
The open-access journal for physics

The temperature-dependent magnetization profile across an epitaxial bilayer of ferromagnetic $La_{2/3}Ca_{1/3}MnO_3$ and superconducting $YBa_2Cu_3O_{7-\delta}$

S Brück[1,2,6], S Treiber[2], S Macke[2], P Audehm[2], G Christiani[3], S Soltan[3,4], H-U Habermeier[3], E Goering[2] and J Albrecht[5]

[1] University of Würzburg, Physikalisches Institut, Am Hubland, D-97074 Würzburg, Germany
[2] Max Planck Institute for Metals Research, Heisenbergstrasse 3, D-70569 Stuttgart, Germany
[3] Max Planck Institute for Solid State Research, Heisenbergstrasse 1, D-70569 Stuttgart, Germany
[4] Physics Department, Faculty of Science, Helwan University, 11792-Cairo, Egypt
[5] Hochschule Aalen, Beethovenstrasse 1, D-73430 Aalen, Germany
E-mail: seb@brueck-online.com

New Journal of Physics **13** (2011) 033023 (15pp)
Received 21 July 2010
Published 18 March 2011
Online at http://www.njp.org/
doi:10.1088/1367-2630/13/3/033023

Abstract. Epitaxial bilayers of ferromagnetic (FM) $La_{2/3}Ca_{1/3}MnO_3$ (LCMO) and superconducting $YBa_2Cu_3O_{7-\delta}$ (YBCO) have been grown on single-crystalline $SrTiO_3$ (STO) substrates by pulsed laser deposition. The manganese magnetization profile across the FM layer has been determined with high spatial resolution at low temperatures by x-ray resonant magnetic reflectivity (XRMR) performed at the BESSY II synchrotron light source of the Helmholtz Zentrum Berlin. It is found that not only the adjacent superconductor but also the substrate underneath influences the magnetization of the LCMO film at the interface at low temperatures. Both effects can be investigated individually by XRMR.

[6] Author to whom any correspondence should be addressed.

Contents

1. Introduction **2**
2. Experimental **2**
3. Results **3**
3.1. Magnetometry magneto-optics 3
3.2. Optical constants 4
3.3. X-ray resonant reflectometry (XRR) and structural characterization 5
3.4. X-ray resonant magnetic reflectometry (XRMR) 6
4. Conclusion **14**
Acknowledgments **14**
References **14**

1. Introduction

The properties of heterostructures made from high-temperature superconductors such as $YBa_2Cu_3O_{7-\delta}$ (YBCO) and spin-polarized ferromagnets such as $La_{2/3}Ca_{1/3}MnO_3$ (LCMO) are strongly influenced by coupling phenomena at the interfaces. In general, superconductivity and ferromagnetism are incompatible ordering principles and their combination leads to substantial competition between the two ordered ground states [1]. In the case of hybrids of high-temperature superconductors and oxide ferromagnets, this usually leads to the suppression of both transition temperatures [2, 3]. Several mechanisms have been discussed to explain this observation, including oxygen diffusion [4], charge transfer due to a discontinuity in the chemical potential [5], a redistribution of the orbital occupancy [6], diffusion of spin-polarized quasiparticles [2, 7] and finally dipolar magnetic coupling via stray fields [8, 9]. In addition to lowered ordering temperatures, magnetic coupling phenomena can be observed in particular in superlattices. For periodic structures of superconductors and ferromagnets with many layers, magnetic coupling between second-nearest neighbours can be found, indicating magnetic coupling via a superconducting (SC) layer [10]. This, however, could be experimentally shown only in superlattices where the SC part consists of $Y_{0.6}Pr_{0.4}Ba_2Cu_3O_{7-x}$ rather than $YBa_2Cu_3O_{7-x}$.

To obtain fundamental understanding of possible magnetic coupling phenomena in hybrid or heterostructures of YBCO and LCMO, we focus in this paper on the simplest possible structure, a bilayer of LCMO and YBCO on a single-crystalline substrate. This system was investigated by x-ray resonant magnetic reflectivity (XRMR), a technique that provides structural and element selective magnetic depth profiles with very high spatial resolution [11]–[13].

Determining the magnetization profile across the ferromagnetic (FM) layer by XRMR we can directly investigate the interaction at the LCMO/YBCO and the LCMO/substrate interface. Both results can act as a prerequisite for the understanding of coupling phenomena in LCMO/YBCO superlattices.

2. Experimental

A $5 \times 5\,mm^2$ $SrTiO_3$ (STO) single crystal with (100) cut and polished surface is used as a substrate. The substrate has been chemically treated [14] to provide a TiO_2 terminated (100)

surface; it was then mounted in a growth chamber with a base pressure of 5×10^{-4} Pa. Bilayers of LCMO and YBCO with a nominal thickness of 400 Å each have been deposited by PLD at a growth temperature of 730 °C at an oxygen pressure of 50 Pa. Full oxygenation has been achieved by annealing the films at 530 °C in an oxygen atmosphere of 10^5 Pa for half an hour and then slowly cooling down to room temperature. These parameters lead to epitaxial growth of LCMO on STO and the resulting LCMO single-layer film with a nominal thickness of 400 Å is an FM metal with a T^{Curie} of 240 K. Subsequently, a 400 Å layer of optimally doped YBCO was grown on top of the LCMO. The SC transition temperature was experimentally derived from an identical sample using superconducting quantum interference device (SQUID) magnetometry and a value of $T_C = 88$ K is found, which verifies the high quality and optimal doping of the layer.

The XRMR and x-ray magnetic circular dichroism (XMCD) measurements were carried out at the undulator beamline UE56/2-PGM1 at the BESSY II light source of the Helmholtz–Zentrum Berlin (HZB), Germany. We used a dedicated soft x-ray magnetic reflectometry end station built at the MPI for Metals Research [15]. This setup allows measuring XRMR curves for angles of incidence of $\theta = 0°$–$70°$. Additionally, high-quality x-ray absorption spectrum (XAS) and XMCD can be measured by total electron yield (TEY) and fluorescence yield (TFY) providing *in situ* spectroscopy data necessary for reflectometry simulations.

In general, it is not possible to obtain the optical profile directly from a measured reflectivity curve. Instead, an iterative approach is used to indirectly obtain the optical profile by fitting a simulated curve to the measurement. Using the simulation software ReMagX, which has been developed specially for this purpose at the MPI for Metals Research [16], we can simulate magnetic reflectivity and asymmetry curves and fit them to the measured reflectivity data. This task is further complicated by the fact that XRMR has to be measured at a magnetic active resonant absorption edge, i.e. a transition that shows circular dichroism (usually $L_{2,3}$ or $M_{4,5}$ edges in the soft x-ray regime). The optical properties at resonant edges show dramatic changes with the energy and the electronic configuration of the elements, e.g. oxidation state [17]. It is therefore imperative to experimentally obtain the optical and magneto-optical constants of the investigated sample [18]. By measuring the near-edge x-ray absorption fine structure (NEXAFS) and also the XMCD for the relevant energy range, the optical and magneto-optical constants can be derived (see e.g. in [19, 20]). This information is then used for the simulation of the XRMR curves while the structural (roughness/thickness) parameters are free parameters for the fitting process. This method ultimately provides element-selective structural and magnetic depth profiles of a layered sample with very high spatial resolution [11]–[13].

3. Results

3.1. Magnetometry magneto-optics

SQUID magnetometry has been used to characterize the bulk magnetic properties of the LCMO/YBCO bilayer at $T = 100$ K, i.e. above the SC transition. To avoid damaging the surface of the sample intended for the XRMR investigation, a sister sample simultaneously prepared in the same run for the deposition has been used for this measurement. The sample was mounted in a Quantum Design MPMS-XL 7T SQUID, cooled from room temperature to $T = 100$ K in zero field, and a magnetic hysteresis was recorded with the magnetic field oriented parallel to the sample surface, i.e. in in-plane geometry. Figure 1 shows the resulting $T = 100$ K

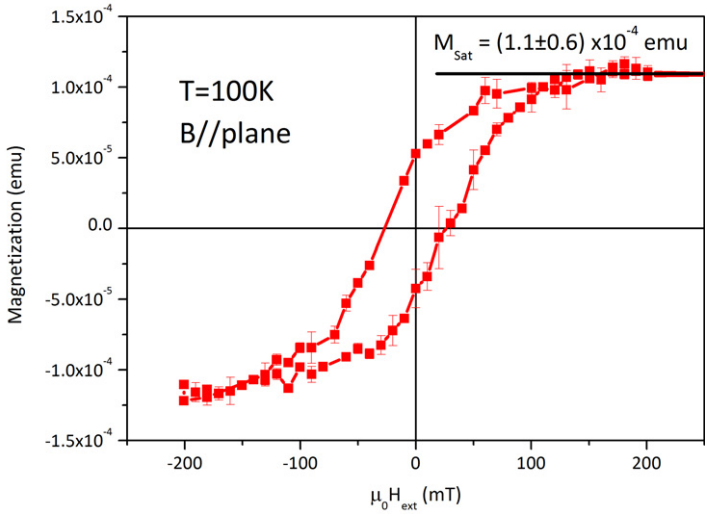

Figure 1. Magnetic in-plane hysteresis measured at $T = 100\,\mathrm{K}$ using a SQUID magnetometer.

hysteresis loop of the sample that has been corrected for the diamagnetic contribution from the STO substrate.

A clear FM hysteresis with a coercive field of $H_C = 25\,\mathrm{mT}$ and a saturation magnetization of $M_{sat} = (1.1 \pm 0.6) \times 10^{-4}\,\mathrm{emu}$ is found. Using a value of 390 Å for the thickness of the LCMO layer as revealed by reflectometry (see below) and taking the lateral film size of $5 \times 5\,\mathrm{mm}^2$ (substrate size) into account, the saturation magnetization is $M_{sat} = 113\,\mathrm{emu\,cm}^{-3}$, which corresponds to a magnetic moment per Mn atom of $0.7\mu_B$. This value is much smaller compared to the bulk magnetization value of $3.7\mu_B$ for LCMO [21]. From previous investigations of LCMO/YBCO bilayers it is known that the magnetic moment of LCMO is affected by the presence and thickness of the YBCO layer [2]. The maximum saturation magnetization of LCMO decreases for increasing YBCO layer thickness and our results are comparable to those of [2].

The SC properties of the YBCO layer were characterized using the magneto-optical Faraday effect. This method uses an iron-garnet indicator film to image the flux line density in the YBCO layer and allows determining the critical current density of the film [22]. A maximal critical current density of $j_s = 7 \times 10^{10}\,\mathrm{A\,m}^{-2}$ is found. Compared to bulk YBCO, this value is reduced by nearly one order of magnitude, which is related to the presence of the ferromagnet [23].

3.2. Optical constants

The energy-dependent optical properties of the individual layers, i.e. the complex indices of refraction $N_j(E) = 1 - \delta(E) + \mathrm{i}\beta(E)$, where j is the layer index, are a necessary prerequisite for the determination of the structural and magnetic depth profile. While the imaginary (absorptive) part, β, is directly accessible from a soft x-ray absorption measurement by fitting the data to tabulated values [24], the real (dispersive) part, δ, can be calculated from β using the Kramers–Kronig relation [19].

An XAS was measured by TEY [25] in the energy range $E = 600$ to $700\,\mathrm{eV}$. Linear polarized x-rays were used for the measurement and the sample was set to an angle of incidence

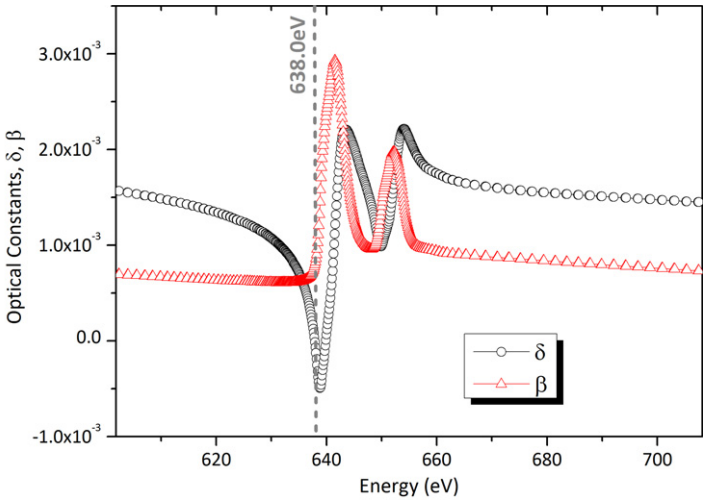

Figure 2. Optical constants for LCMO in the vicinity of the Mn $L_{2,3}$ edges derived by measuring an XAS and applying a Kramers–Kronig transform (see details in the text). The indicated energy of $E = 638$ eV was used for the XRMR investigation. As can be seen, the dispersion dominates at this energy, while the imaginary part of the index of refraction is still small.

of $\theta = 45^\circ$. The resulting spectrum was then adapted to tabulated x-ray scattering factors [24] to obtain the imaginary part of the scattering factor f_2 including the sample specific $L_{2,3}$ edge resonances. A Kramers–Kronig transform similar to the one described in [19] was used to calculate the real part f_1. Finally, the optical theorem [26] links the optical constants δ and β to the forward scattering cross sections f_1 and f_2 according to $\delta(E) = \frac{N_A \rho}{A} \frac{r_0 \lambda^2}{2\pi} f_1(E)$ and $\beta(E) = \frac{N_A \rho}{A} \frac{r_0 \lambda^2}{2\pi} f_2(E)$. Here, r_0 is the classical electron radius, N_A is the Avogadro constant, A is the atomic mass number (mass mol^{-1}), ρ is the mass density (mass vol^{-1}) and λ is the wavelength of the incident x-rays. The results are shown in figure 2 for the energy range close to the Mn $L_{2,3}$ edges.

For the calculation of δ and β from f_1 and f_2, it was assumed that the stoichiometry of the LCMO layer is exactly $La_{2/3}Ca_{1/3}MnO_3$. The validity of this assumption will later be confirmed by the high quality of the structural reflectometry fits presented below. The indicated energy of $E = 638$ eV is used for all subsequent XRMR measurements. This particular energy provides a large scattering cross section (δ is maximal) and nearly no resonant enhancement of the absorption. The optical constants of the YBCO layer and the STO substrate were directly retrieved from tabulated values [24]. This is justified since all soft x-ray resonant edges in these materials (Cu, Ba and O) are far away from the energy where the XRMR is measured.

3.3. X-ray resonant reflectometry (XRR) and structural characterization

XRR and XRMR are used to investigate the structural properties, i.e. layer thicknesses and roughness, of the bilayer system and the magnetic depth profile of the LCMO layer. The structural/chemical depth profile of the sample is obtained by measuring non-magnetic resonant reflectivity (XRR) curves, i.e. resonant reflectivity without XMCD contrast, and fitting a simulation to them. It is favourable to measure XRR and XRMR at the same energy because it allows using the results from XRR directly as input for the XRMR. The structural depth profile

is determined by the layer thicknesses, the interface roughness and the chemical composition. The chemical composition was used as a fixed input parameter (nominal compositions), while the roughness and thicknesses of all layers and the substrate were set as free parameters of the fitting process.

We use the dedicated software tool 'ReMagX' [16] for simulation and fitting of the reflectivity data. ReMagX uses a 4×4 matrix formalism [27] that allows simulating the reflectivity from an arbitrary magnetic layer stack. Whereas standard reflectometry for optical isotropic media uses the Parratt formalism [28] for simulation, this technique has shortcomings for the resonant magnetic data presented here since it neglects the optical anisotropic nature of the XMCD effect. Therefore ReMagX calculates the full polarization-dependent eigenfunctions for each layer and thus accounts for the anisotropy and any intensity transfer. Interface roughness and local variations of the magneto-optical properties and hence the magnetic moment are incorporated into the matrix description by modelling the profile by thin slices [16, 29]. The local variations of the magneto-optical constants can be introduced by Gaussian profiles with a variable position, full-width at half-maximum (FWHM) and height. This either modifies an existing magnetic moment, i.e. magneto-optical contribution, or it introduces a new, artificial magnetic signal. ReMagX provides several fitting algorithms for fitting the simulation to the measured data. Simplex, Levenberg–Marquardt, Simplex with simulated annealing and a nonlinear optimization based on a genetic algorithm are available. Whereas the former three use a standard χ^2 test as a measure of the quality of the fit, the genetic algorithm uses a weighted χ^2 as fitness function $F = \sum(x - y)^2 / \sum(x^2 + y^2)$ according to Tiilikainen *et al* [30]. Note that for reflectivity data, the logarithm of x and y is used. More details and also restrictions on the XRMR data processing and can be found in e.g. [17]–[19], [31]–[33].

Figure 3 shows the resonant non-magnetic reflectivity measured at $T = 110\,\mathrm{K}$ at an x-ray energy of $E_{hv} = 638\,\mathrm{eV}$ using linear horizontally polarized light along with the best simulation result (red solid curve) obtained from fitting the data.

The simulation perfectly reproduces the measured reflectivity curve in the range from $q_z = 0.08$ to $0.275\,\mathrm{Å}^{-1}$ where the relevant, structure-determined features are located. The deviation for small angles is related to the incomplete illumination of the sample. The non-magnetic reflectivity was also measured for $T = 300$ and $40\,\mathrm{K}$ to verify that the chemical structure does not change with temperature. A close-up of all three measured curves in the range from $q_z = 0.0625$ to $0.2\,\mathrm{Å}^{-1}$ is shown in the inset of figure 3 together with the corresponding simulation results.

From the simulation shown in figure 3, the optical depth profile, which corresponds to the structural depth profile, is derived and the result is shown in figure 4.

A thickness of $(390 \pm 2)\,\mathrm{Å}$ and $(403 \pm 5)\,\mathrm{Å}$ is found for the LCMO and YBCO layers, respectively. Both interfaces are very smooth showing an RMS roughness of $(9.5 \pm 0.1)\,\mathrm{Å}$ for the LCMO/YBCO interface and only $1\,\mathrm{Å}$ for the STO/LCMO interface. The errors were derived from comparing the three temperatures measured. The validity of the chemical composition model was tested by comparing simulations based on the above profile to measurements at other energies (Mn L_2, Cu L_3, data not shown).

3.4. X-ray resonant magnetic reflectometry (XRMR)

A series of temperature-dependent XRMR curves were measured for θ ranging from $\theta = 0^\circ$ to 27.75° (corresponding to $q_z = 0$ to $0.3\,\mathrm{Å}^{-1}$) in an applied external magnetic field of

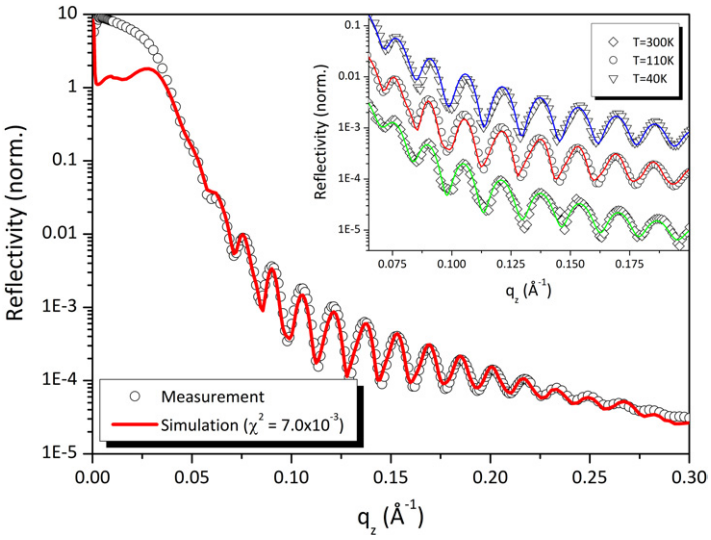

Figure 3. Resonant XRR curve without magnetic contrast measured at $T = 110\,\mathrm{K}$ using an x-ray energy of 638 eV and linear horizontally polarized light. The red curve is the best-fit result ($\chi^2 = 7.0 \times 10^{-3}$). The inset shows a close-up of the curve for $q_z = 0.0625$–$0.2\,\mathrm{Å}^{-1}$ together with the results obtained at $T = 40\,\mathrm{K}$ ($\chi^2 = 6.0 \times 10^{-3}$) and $T = 300\,\mathrm{K}$ ($\chi^2 = 5.1 \times 10^{-3}$). Note that the curves have been shifted vertically for better readability. No significant change in the non-magnetic reflectivity and therefore also the underlying chemical structure is found.

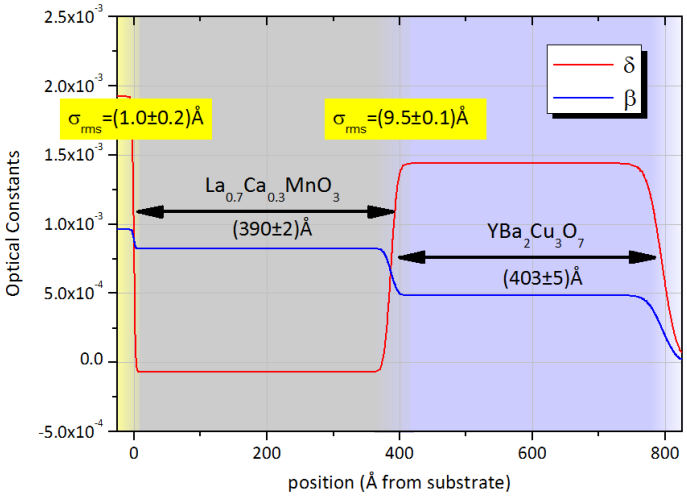

Figure 4. Optical, i.e. structural, depth profile of the sample measured at an x-ray energy of $E = 638\,\mathrm{eV}$ and a temperature of $T = 110\,\mathrm{K}$.

$H_{\mathrm{ext}} = 130\,\mathrm{mT}$ parallel and antiparallel to the sample surface (in-plane geometry). X-rays with an energy of $E = 638\,\mathrm{eV}$ (Mn L_3 edge) with positive helicity were used and the external magnetic field was flipped at every angle from parallel to antiparallel alignment (with respect to the beam direction). The intensity of the specular reflection was measured for each angle and

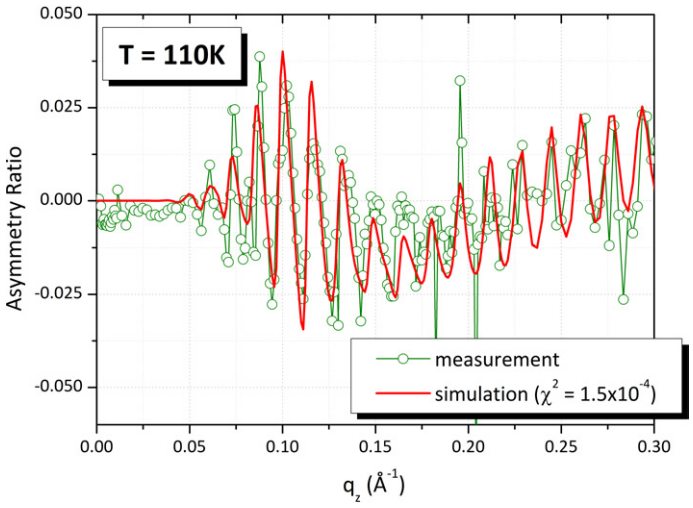

Figure 5. Element-selective Mn asymmetry ratio between $R^{\uparrow\uparrow}$ and $R^{\uparrow\downarrow}$ measured at an energy of $E = 638\,\text{eV}$. The curve is the average of the positive and negative helicity measurements. The red solid curve represents the best-fit result ($\chi^2 = 5.1 \times 10^{-3}$) based on the magneto-optical profile shown in figure 6.

field direction. Subsequently, the same measurement was repeated for negative helicity of the x-rays.

To extract the magnetic signal from the two dichroic curves, the asymmetry ratio between the two is calculated according to $A = \frac{R^{\uparrow\uparrow} - R^{\uparrow\downarrow}}{R^{\uparrow\uparrow} - R^{\uparrow\downarrow}}$. Here the first arrow indicates the helicity of the x-rays ($\uparrow$= positive and $\downarrow$= negative circular polarized light) and the second arrow indicates the direction of the external magnetic field ($\uparrow$= positive and $\downarrow$= negative) with respect to the direction of the incident x-rays.

First the magnetic asymmetry signal associated with Mn was measured at a temperature of $T = 110\,\text{K}$, which is well above the SC transition temperature. Figure 5 shows the resulting asymmetry ratio together with the best simulation result obtained from fitting the data.

A small asymmetry ratio of the order of 2.5% is found originating from FM Mn in the LCMO layer. This asymmetry ratio exhibits two major features: A short-range oscillation that is mostly related to the YBCO thickness and a long-range modulation that should originate from a smaller structure in the magneto-optical profile. Analysing the short-range oscillation yields $\Delta q_z = 0.0158\,\text{Å}^{-1}$, which corresponds to a thickness of 397 Å. This value corresponds, within the error, to the structural properties of the YBCO layer (compare figure 4). To obtain the magneto-optical profile connected with the asymmetry signal, the data have been fitted [16] and the fit result is also shown in the plot as a red solid curve. The fit reproduces very well the major features of the asymmetry very good. The fitting process consists of two steps: first the magneto-optical constants for LCMO were derived from XMCD data of FM LCMO and rescaled to account for the reduced magnetic moment of Mn in this sample (see section 3.1). In a second step, the magneto-optical constants were used to fit the asymmetry signal while allowing local variations (enhancement or suppression) of the magneto-optical profile and hence the saturation magnetization. The result is shown as inset in figure 6.

The overall shape of the asymmetry ratio, especially the long-range modulation, can only be reproduced if a layer with reduced or completely suppressed magnetization close to the

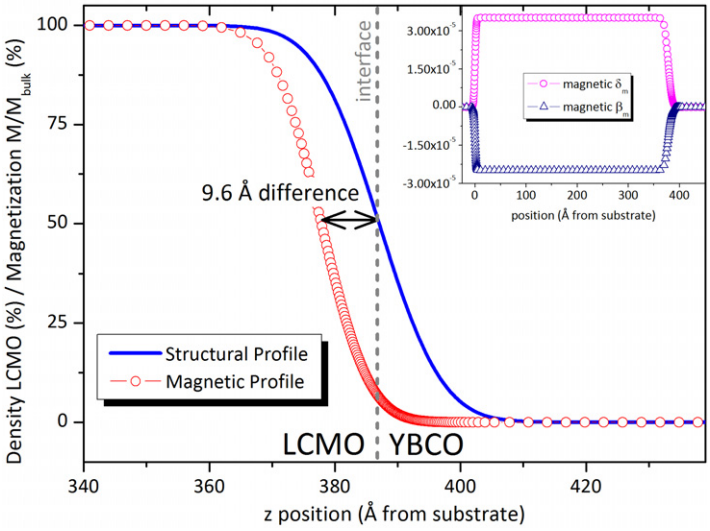

Figure 6. Magnified structural and magnetic profiles close to the LCMO/YBCO interface. Note both graphs were normalized to the bulk optical and magneto-optical values of the LCMO layer. The magnetic profile sets in roughly 10 Å beneath the structural transition and the magnetic moment close to the interface is strongly reduced. The inset to the upper right shows the absolute overall magneto-optical profile for the LCMO layer.

YBCO is inserted into the magneto-optical profile. Compared to the overall thickness of the LCMO film, this feature is quite narrow. Therefore, figure 6 shows a close-up of the interface region between LCMO and YBCO, while the full magneto-optical profile is shown as inset in the same figure.

Here the Mn density (blue) and the magnetic signal (red open circles) are plotted in per cent with respect to the bulk layer properties. The magnetic profile is shifted compared to the structural interface by 9.6 Å, which means that the LCMO directly at the interface to the YBCO has a reduced or zero magnetic moment. Note that the small asymmetry makes it difficult to derive the exact magnetization at the interface. Therefore we cannot exclude a small remaining moment for the LCMO directly at the interface; the magnetic signal in figure 6 can still refer to an FM-ordered state but with a strongly suppressed magnetization value.

Figure 7 depicts an analogue measurement to figure 5, now at a temperature of $T = 40\,\mathrm{K}$, much below the SC transition of the YBCO layer. Similar to the high temperature data, we can simulate the asymmetry nearly perfectly ($\chi^2 = 1.8 \times 10^{-4}$) by our algorithm.

We find a striking difference between the results at $T = 110\,\mathrm{K}$ and 40 K, respectively. The asymmetry curve at $T = 40\,\mathrm{K}$ exhibits a clear increase at q_z values of $q_z = 0.2\,\mathrm{Å}^{-1}$ and above. A wide maximum seems to occur for high momentum transfer. Since the observed reflectometry oscillations refer to inverse length scales as in reciprocal space, a wide maximum refers to a narrow structure in the magnetization profile. Moreover, the fact that this effect occurs at large q_z values directly indicates that this feature has to be buried at a great depth under the surface.

Our algorithm again allows the determination of the corresponding magnetic profile that is depicted in figure 8. At a temperature of $T = 40\,\mathrm{K}$ a new feature of the magnetization profile across the LCMO layer is found. A sharp peak where the local magnetization is roughly doubled

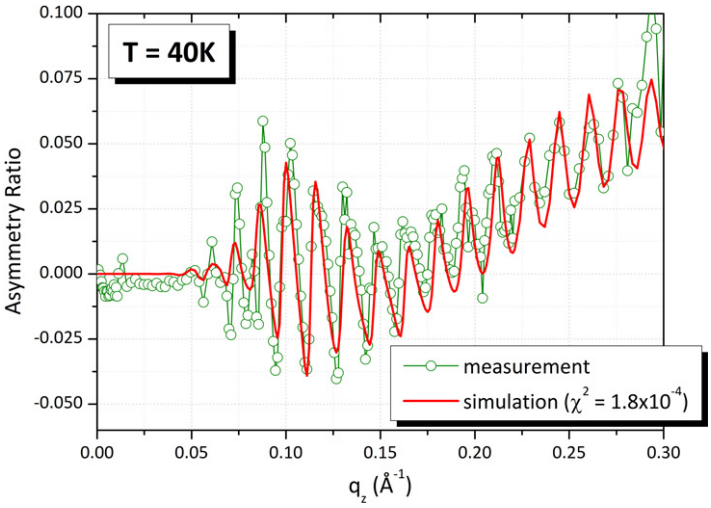

Figure 7. Magnetic asymmetry ratio measured at $T = 40$ K and an x-ray energy of 638 eV.

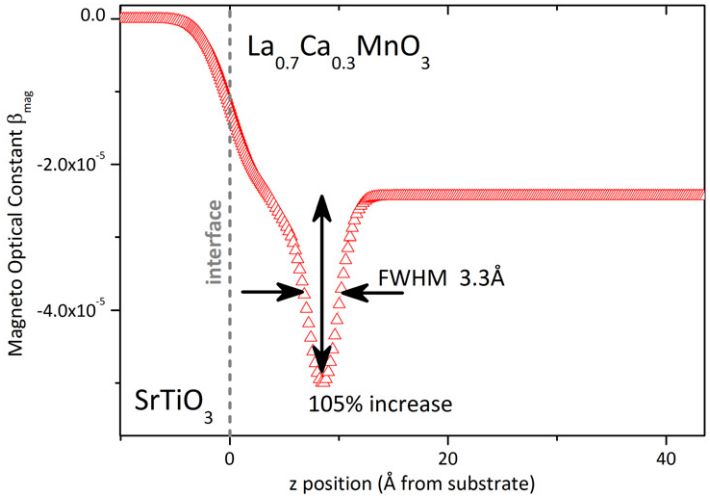

Figure 8. Magneto-optical profile for the absorptive part of the index of refraction in the vicinity of the LCMO/STO interface obtained for the $T = 40$ K asymmetry. The magneto-optical constants are both increased by more than 100%, which indicates an increase of the manganese magnetic moment per atom to $1.44\mu_B$ with respect to the SQUID-derived bulk value.

is found close to the interface to the substrate. Obviously there is an interaction between the LCMO film and the STO substrate at low temperatures leading to an additional magnetic effect. The presence of a magnetization increase close to the substrate in a YBCO/LCMO superlattice was already reported from neutron scattering [34]. We confirm this finding and show in the following an analysis of the temperature dependence of the effect providing deeper insights into its origin.

To further discuss the two main findings that are the suppressed magnetization at the interface to YBCO and the temperature-dependent increase at the interface to STO, we

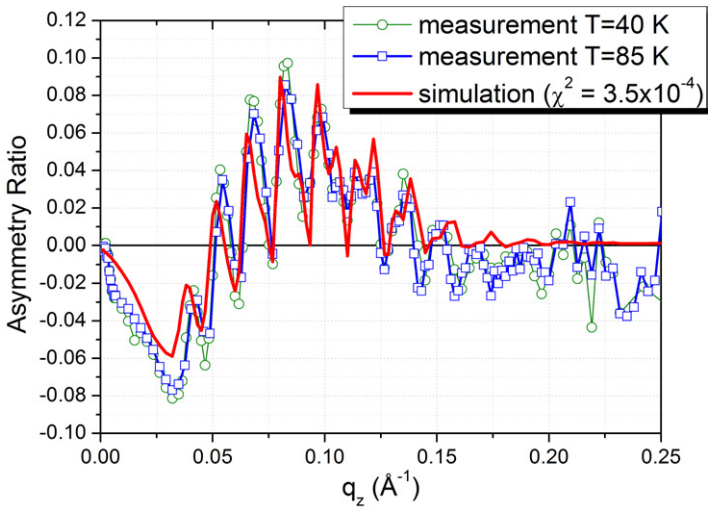

Figure 9. Element-selective Mn asymmetry ratio of a YBCO/LCMO bilayer (reversed stacking) measured at an energy of $E = 635$ eV for $T = 85$ and 40 K. In contrast to the LCMO/YBCO layer (see figures 5 and 8), no temperature dependence of the asymmetry occurs. The red solid curve represents the best-fit result ($\chi^2 = 3.5 \times 10^{-4}$), which reveals a layer of suppressed LCMO magnetization at the interface to the YBCO (∼10 Å) and at the surface (∼20 Å).

performed an analogous analysis to figures 5 and 7 at additional temperatures and also for a bilayer sample with reversed stacking (YBCO/LCMO).

Similar measurements to those shown above were performed on a YBCO/LCMO bilayer, i.e. a bilayer with reversed stacking, to check whether the observed suppression at the interface to YBCO is of general character for bilayers or whether it depends on the stacking sequence of the layers. The growth conditions of this sample were identical to the LCMO/YBCO sample. The YBCO/LCMO bilayer exhibits a reduced SC transition temperature of $T_C = 65$ K and therefore XRMR was measured for temperatures of $T = 85$ and 40 K and at an energy of $E = 635$ eV using the same experimental parameters as for the LCMO/YBCO sample. The data processing was carried out in the same way as described above and the resulting asymmetry ratios are shown in figure 9. Before analysing the magnetic asymmetry ratio, the roughnesses and thicknesses of the layers were derived from the non-magnetic reflectivity signal in an analogue way as for the LCMO/YBCO bilayer. An LCMO thickness of (370 ± 4) Å and a YBCO thickness of 361 Å are found. The interface between the YBCO layer and the LCMO on top exhibits an rms roughness of 11 Å.

Although the measurements were carried out well in front of the magnetic-sensitive L_3 edge, a clear magnetic asymmetry of up to 10% is found at $E = 635$ eV which is related to the real part of the magneto-optical constants. No difference occurs in the magnetic asymmetry of the LCMO when cooling from $T = 85$ K to $T = 40$ K. This result is in strong contrast to the behaviour of the LCMO/YBCO bilayer (see figures 5, 7 and 10), which shows a strong temperature-dependent asymmetry. The measured asymmetry at $T = 40$ K was fitted using the same optical and magneto-optical constants and the best-fit result is shown in figure 9 as a red solid line. The fitting process leads to a magnetic depth profile with two regions with suppressed magnetization within the LCMO layer. Similar to the LCMO/YBCO bilayer,

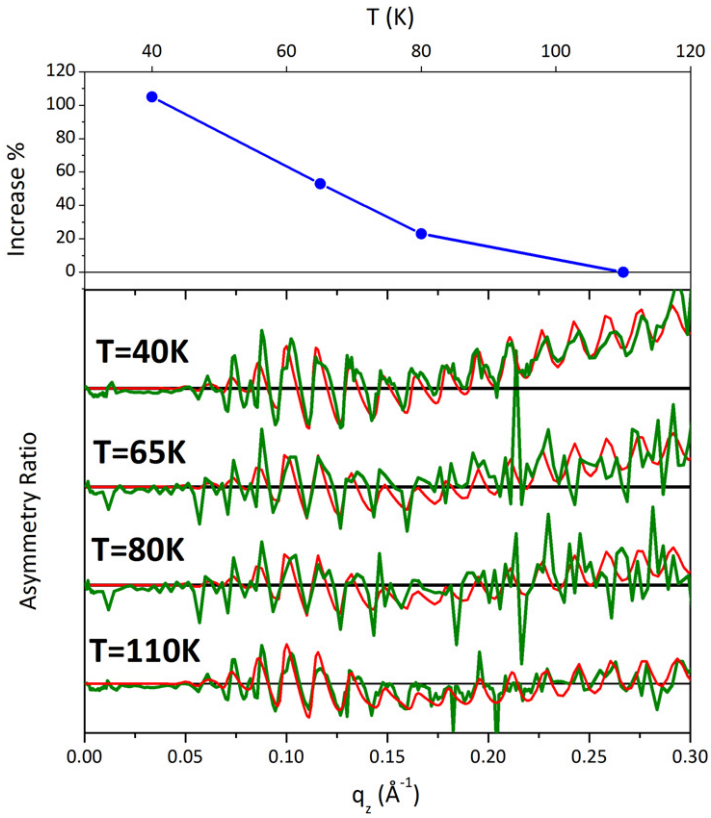

Figure 10. Temperature dependence of the increased Mn magnetic moment close to the STO interface. The lower part shows all measured asymmetry curves along with the corresponding fit results ($\chi^2 = 1.8 \times 10^{-4}$, 6.0×10^{-4}, 5.7×10^{-4} 1.5×10^{-4} for $T = 40$, 65, 80 and 110 K, respectively). The upper section shows the per cent increase of the Mn magnetization at the STO interface (see figure 8) derived from the simulation curves.

the YBCO/LCMO sample exhibits a ∼10 Å broad layer of suppressed magnetization at the interface to the YBCO. Additionally, the LCMO layer has a suppressed magnetic moment in a ∼20 Å wide region close to the sample surface. The latter is likely related to a growth-induced breakdown of the oxygen stoichiometry and will be subject to future investigations.

The existence of a layer of suppressed LCMO magnetization at the interface to YBCO was already reported for some FM/SC superlattices [35, 36]. Our results show that a suppressed layer already occurs at a single FM/SC interface and does not depend on the SC state of the YBCO in the bilayer system since it is already present at $T = 110$ K for the LCMO/YBCO bilayer ($T = 85$ K for the YBCO/LCMO bilayer). The latter observation is consistent with the results from superlattices [36] and with magnetization measurements of YBCO/LCMO bilayers, which clearly show a YBCO thickness-related decrease of the LCMO saturation moment already well above the SC transition (see figure 6 in [2]).

In contrast to the results presented here and in [35, 36], a uniform magnetization of the LCMO layer, i.e. no suppression at the interface, was also found in superlattices [6, 10]. A possible explanation for the contradictory results might be related to the roughness of the LCMO/YBCO interface in both bilayers. There is a striking coincidence of the interface

roughness as revealed by x-ray reflectometry and the shift of the structural and magnetic profiles (see figure 6). For the LCMO/YBCO bilayer the interface roughness is $\sigma_{\mathrm{rms}} = 9.5$ Å and the shift 9.6 Å, while for YBCO/LCMO bilayer the roughness is 11.2 Å with a shifted onset of magnetization of 10.6 Å. This interface roughness—substantially larger than in the YBCO/LCMO superlattices [6, 10]—could be accounted for by the suppression of the magnetization at the interface. A charge transfer from YBCO to LCMO, as suggested [36, 37] to explain the occurrence of magnetic dead layers in LCMO/YBCO superlattices grown by oxygen high-pressure sputtering, might occur in this broad interface region and would explain the observed effect. However, roughness in reflectometry does not distinguish between diffusion and unit cell steps or even larger in-plane structures. Therefore, it is very difficult to identify the origin of the suppressed magnetization in LCMO directly from the data presented here.

For a quantitative statement concerning the magnetization increase in the LCMO/YBCO bilayer, the asymmetry curves at $T = 40$, 65, 80 and 110 K have been fitted and the results are plotted in figure 10.

All four temperatures can be fitted using the same general shape of the magneto-optical profile close to the STO interface (compare figure 8). The increased noise level of the $T = 65$ and 80 K measurements is related to a reduced integration time for these measurements. Nevertheless the general trend is clearly visible from the curves and can be fitted successfully. We clearly see that the effect continuously decreases with increasing temperature and seems to vanish around $T = 100$ K.

The observed temperature dependence of the LCMO–substrate interaction is tentatively considered to be related to the structural properties of STO single crystals at low temperatures. STO has a lattice parameter of 3.905 Å at room temperature, whereas LCMO has only 3.867 Å [38]–[40]. This 1% lattice mismatch causes tensile strain in an LCMO thin film grown on STO and is responsible for the reduced magnetic moment of such films [39]–[42]. However, if the sample is cooled down, the lattice parameter of STO decreases continuously [38, 43]. The structural phase transition from cubic to tetragonal that occurs below $T = 105$ K ([38], [43]–[45]) results in an even faster decrease of the in-plane lattice parameter, leading to less tensile strain in the LCMO film.

The correlation of the increased magnetization in the LCMO with the structural change of the STO is supported by the fact that the sample with reversed stacking, where the LCMO is grown on top of YBCO, does not show any change between $T = 85$ and 40 K (see figure 9). We propose a scenario where the growth-induced tensile strain from the substrate [40] and the compressive strain caused by the presence of the YBCO layer [2] create a thickness-dependent state of stress in the LCMO layer, which is responsible for the reduced magnetic moment in the bulk observed here. The tetragonal distortion of the STO, i.e. the change of the in-plane lattice parameter, below $T = 105$ K disturbs this balance and allows a relaxation of the first few monolayers of the LCMO, which causes a local increase of the saturation moment from about $0.7\mu_{\mathrm{B}}$ to $1.4\mu_{\mathrm{B}}$ per Mn atom.

The reason why this effect, which should be of general character for LCMO films grown on STO, was not yet observed for pure LCMO layers is related to the different experimental methods used. Most investigations used samples with a static strain, e.g. by using different substrates or by varying the layer thickness. Moreover, the results were obtained by using standard magnetometry, which measures the whole film and not a local variation of it. The investigation presented here is very different in two important points: the XRMR technique

detects even small localized changes of the magnetization profile. In the present case, the observed increase at the LCMO/STO interface is less than 1% (for $T = 40$ K) of the total LCMO magnetic moment. Such a small signal is hard to detect with standard, bulk-sensitive magnetometry. The second important difference is that the increase of magnetization observed in the present work is reversible. The measurement sequence was 40 K → 110 K → 65 K → 80 K and the effect is visible at $T = 40$ K, then vanishes at $T = 110$ K and comes back when cooling again to 65 K (see figure 9). This implies that a reversible mechanism like the strain-induced effect that we propose here has to be responsible for the increase of magnetic moment at the interface. Cation segregation as it was observed by electron energy loss spectroscopy of LCMO thin films [46] cannot explain this behaviour since segregation is a growth-induced effect and should therefore not be reversible by cooling or heating in this temperature range.

4. Conclusion

In conclusion, we have found that the magnetization profile across FM LCMO layers in bilayers of LCMO/YBCO and YBCO/LCMO on STO substrates is strongly affected by the interfaces to the adjacent materials. A suppression of the LCMO magnetization close to the YBCO layer on a length scale of 10 Å is found at all temperatures and for both stacking sequences. The transition to superconductivity in the YBCO seems not to influence this finding. A second effect occurs at the LCMO/STO interface at low temperatures. Owing to the structural change of the in-plane lattice parameter of STO single crystals, a peak-like magnetization increase develops inside the LCMO layer close to the substrate interface, which has its origin in reduced tensile strain arising from the STO substrate.

Acknowledgments

We are indebted to B Keimer, E Benckiser and V Hinkov for helpful discussions. Support by B Zada, W Mahler and the whole HZB-BESSY II team during the beamtime is gratefully acknowledged. SB thanks to the Helmholtz Zentrum Berlin (HZB) for financial support.

References

[1] Sá de Melo C A R 1997 *Phys. Rev. Lett.* **79** 1933
[2] Soltan S, Albrecht J and Habermeier H-U 2004 *Phys. Rev.* B **70** 144517
[3] Sefrioui Z, Arias D, Peña V, Villegas J E, Varela M, Prieto P, León C, Martinez J L and Santamaria J 2003 *Phys. Rev.* B **67** 214511
[4] Chakalov R A, Passerieux G, Jones I P, Mikheenko P, Ireland J, Chakalova R I, Colclough M S and Muirhead C M 2005 *J. Appl. Phys.* **98** 123908
[5] Varela M, Lupini A R, Pennycook S J, Sefrioui Z and Santamaria J 2003 *Solid-State Electron.* **47** 2245–8
[6] Chakhalian J *et al* 2006 *Nat. Phys.* **2** 244–8
[7] Habermeier H-U, Soltan S and Albrecht J 2007 *Phys. C: Supercond.* **460–462** 32–5
[8] Albrecht J, Soltan S and Habermeier H-U 2005 *Phys. Rev.* B **72** 092502
[9] Albrecht J, Djupmyr M, Soltan S, Habermeier H-U, Connolly M R and Bending S J 2007 *New J. Phys.* **9** 379
[10] Hoppler J *et al* 2009 *Nat. Mater.* **8** 315–9
[11] Brück S, Schütz G, Goering E, Ji X and Krishnan K M 2008 *Phys. Rev. Lett.* **101** 126402
[12] Roy S *et al* 2005 *Phys. Rev. Lett.* **95** 047201

[13] Tonnerre J M, De Santis, Grenier S, Tolentino H C N, Langlais V, Bontempi E, Garcia-Fernandez M and Staub U 2008 *Phys. Rev. Lett.* **100** 157202
[14] Koster G, Kropman B L, Rijnders G J H M, Blank D H A and Rogalla H 1998 *Appl. Phys. Lett.* **73** 2920
[15] Brück S, Bauknecht S, Ludescher B, Goering E and Schütz G 2008 *Rev. Sci. Instrum.* **79** 083109
[16] Macke S, Brück S and Goering E 2010 *ReMagX-X-Ray Magnetic Reflectivity Tool* (Stuttgart: Max Planck Institute for Metals Research)
[17] Schütz G, Goering E and Stoll H 2007 *Handbook of Magnetism and Advanced Magnetic Materials* vol 3 ed H Kronmüller and S S P Parkin (New York: Wiley) pp 1309–64
[18] Fähnle M, Steiauf D, Martosiswoyo L, Goering E, Brück S and Schütz G 2007 *Phys. Rev.* B **75** 144415
[19] Brück S, Macke S, Goering E, Ji X, Zhan Q and Krishnan K M 2010 *Phys. Rev.* B **81** 134414
[20] Brück S 2009 Magnetic resonant reflectometry on exchange bias systems *PhD Thesis* Universität Stuttgart
[21] Coey J M D, Viret M and von Molnár S 1999 *Adv. Phys.* **48** 167
[22] Jooss Ch, Albrecht J, Kuhn H, Leonhardt S and Kronmüller H 2002 *Rep. Prog. Phys.* **65** 651–788
[23] Djupmyr M, Soltan S, Habermeier H-U and Albrecht J 2009 *Phys. Rev.* B **80** 184507
[24] Chantler C T 2000 *J. Phys. Chem. Ref. Data* **29** 597–1056
[25] Gudat W and Kunz C 1972 *Phys. Rev. Lett.* **29** 169
[26] Jackson J 1999 *Classical Electrodynamics* 3rd edn (New York: Wiley)
[27] Zak J, Moog E R, Liu C and Bader S D 1991 *Phys. Rev.* B **43** 6423
[28] Parratt L G 1954 *Phys. Rev.* **5** 359
[29] Stepanov S A and Köhler R 1994 *J. Appl. Phys.* **76** 7809–15
[30] Tiilikainen J, Tilli J-M, Bosund V, Mattila M, Hakkarainen T, Airaksinen V-M and Lipsanen H 2007 *J. Phys. D: Appl. Phys.* **40** 215–8
[31] Geissler J, Goering E, Weigand E and Schütz G 2002 *Z. Met. kd.* **93** 946–52
[32] Lee D R, Sinha S K, Haskel D, Choi Y, Lang J C, Stepanov S A and Srajer G 2003 *Phys. Rev.* B **68** 224409
[33] Stepanov S A and Sinha S K 2000 *Phys. Rev.* B **61** 15302
[34] Peña V, Sefrioui Z, Arias D, Leon C, Santamaria J, Martinez J L, teVelthuis S G E and Hoffmann A 2005 *Phys. Rev. Lett.* **94** 057002
[35] Stahn J *et al* 2005 *Phys. Rev.* B **71** 140509
[36] Hoffmann A, te Velthuis S G E, Sefrioui Z, Santamaría J, Fitzsimmons M R, Park S and Varela M 2005 *Phys. Rev.* B **72** 140407
[37] Varela M, Lupini A R, Pena V, Sefrioui Z, Arslan I, Browning N D, Santamaria J and Pennycook S J 2005 arXiv:cond-mat/0508564
[38] Loetzsch R, Lübcke A, Uschmann I, Förster E, Große V, Thuerk M, Koettig T, Schmidl F and Seidel P 2010 *Appl. Phys. Lett.* **96** 071901
[39] Praus R B, Gross G M, Razavi F S and Habermeier H-U 2000 *J. Magn. Magn. Mater.* **211** 41–6
[40] Campillo G, Berger A, Osorio J, Pearson J E, Bader S D, Baca E and Prieto P 2001 *J. Magn. Magn. Mater.* **237** 61–8
[41] de Andrés A, Rubio J, Castro G, Taboada S, Martínez J L and Colino J M 2003 *Appl. Phys. Lett.* **83** 713
[42] Infante I C, Sánchez F, Fontcuberta J, Wojcik M, Jedryka E, Estradé S, Peiró F, Arbiol J, Laukhin V and Espinós J P 2007 *Phys. Rev.* B **76** 224415
[43] Alefeld B 1969 *Z. Phys.* A **222** 155–64
[44] Müller K A, Berlinger W and Waldner F 1968 *Phys. Rev. Lett.* **21** 814
[45] Doi S and Takahashi I 2000 *Phil. Mag.* A **80** 1889
[46] Estradé S, Arbiol J, Peiró F, Infante I C, Sánchez F, Fontcuberta J, de la Peña F, Walls M and Colliex C 2008 *Appl. Phys. Lett.* **93** 112505